**SUPPLEMENTAL MATERIALS**

# Streamlined architecture and GPI-dependent trafficking in the early secretory pathway of African trypanosomes.

Elitza S. Sevova and James D. Bangs

## REFERENCES:

Bi, X., Corpina, R., and Goldberg, J. (2002). Structure of the Sec23/24-Sar1 pre-budding complex of the COPII vesicle coat. Nature *419*, 271-277.

Miller, E.A., Beilharz, T.H., Malkus, P.N., Lee, M., Hamamoto, S., Orci, L., and Schekman, R. (2003). Multiple cargo binding sites on the COPII subunit Sec24p ensure capture of diverse membrane proteins into transport vesicles. Cell *114*, 497-509.

Mossessova, E., Bickford, L., and Goldberg, J. (2003). SNARE selectivity of the COPII coat. Cell *114*, 483-495.

## TABLES:

**Table S1. *T. brucei* COPII Coat Orthologues**

| TbSec Orthologues | Query Input (from *S. cerevisiae)* | BLASTp Value | GeneDB[1] Accession # |
|---|---|---|---|
| TbSar1 | YPL218W | $2.4e^{-56}$ | Tb05.5k5.150 |
| TbSec23.1 | YPR181C | $2.1e^{-113}$ | Tb927.8.3660 |
| TbSec23.2 | YPR181C | $1.7e^{-135}$ | Tb10.6k15.2840 |
| TbSec24.1 | YIL109C | $9.9e^{-65}$ | Tb927.3.1210 |
| TbSec24.2 | YIL109C | $1.7e^{-62}$ | Tb927.3.5420 |
| TbSec13.1 | YLR208W | $3.2e^{-52}$ | Tb10.61.2630 |
| TbSec13.2[2] | YLR208W | $1.6e^{-16}$ | Tb11.01.0420 |
| TbSec31 | YDL195W | $3.3e^{-38}$ | Tb11.02.4040 |

1. http://www.genedb.org/.
2. Protein alignment of this protein to the yeast orthologue suggests it to be a true TbSec13 homologue.

**Table S2. Putative *T. brucei* p24 Orthologues[1]**

| *T. brucei* Orthologue[2] | GeneDB[3] Accession # | Similarity to ScEmp24p[4] | Similarity to ScErv25p[5] | Closest *T. brucei* Paralogue[6] |
|---|---|---|---|---|
| TbERP1 | Tb11.01.6880 | 7.4e-16 | 6.4e-10 | TbERP2 (7.8e-12) |
| TbERP2 | Tb09.244.2760 | 1.4e-5 | 4.7e-14 | TbERP1 (3.3e-13) |
| TbERP3 | Tb927.8.8030 | 3.3e-7 | n.d. | TbERP4 (5.2e-54) |
| TbERP4 | Tb927.4.4350 | 6.1e-6 | 5.3e-5 | TbERP3 (3.2e-47) |
| TbERP5 | Tb927.7.3600 | n.d. | n.d. | TbERP1 (4.1e-7) |
| TbERP6 | Tb10.6k15.1130 | n.d. | n.d. | TbERP1 (1.4e-4) |

1. All genes products are predicted to be small (203-232 residue) Type I transmembrane proteins with short cytoplasmic domains. All are recognized as related to the EMP-GP25L Superfamily by the Pfam database (http://pfam.sanger.ac.uk/).
2. *T. brucei* Emp24 Related Proteins. Arbitrary numbering.
3. http://www.genedb.org/.
4. Query with *S. cerevisiae* Emp24, Accession # CAA96912, BlastP value.
5. Query with *S. cerevisiae* Erv25, Accession # NP_013701, BlastP value.
6. Number in parentheses is BlastP value of *T. brucei* database search.

**FIGURE LEGENDS:**

**Figure S1. Validation of three-dimensional precision of epifluorescent imaging.** BSF cells were co-stained with mouse anti-BiP (B) and rabbit anti-BiP (C) antibodies to detect the ER. The corresponding merged DAPI/DIC image, indicating the nucleus and kinetoplast, is shown in Panel A. The three-channel summed stack projection is shown in Panel D with associated x-z and y-z transects. Marginal hatch marks in the x-z image indicate the planes at which the z-y and z-x transects were captured. This set of images confirms the pixel precise co-localization abilities of our system (see Material and Methods) in the x, y and z-planes.

**Figure S2. Silencing of TbSec subunits has minimal effect on trafficking of endogenous non-GPI anchored reporters.** RNAi silencing of TbSec subunits as indicated (A-D) was induced for 12 hours, and the trafficking of endogenous *Tbb*CATL (top row) and p67 (bottom row) in control (open circles) and silenced cells (closed circles) was assayed as in Figure 1. The rates of turnover were quantified (mean ± s.e.m. for triplicate independent experiments) as disappearance of the initial forms for trypanopain (I + X) and for p67 (gp100).

**Figure S3. Domain organization and sequence alignments of the *S. cerevisiae* and *T. brucei* Sec23/Sec24 orthologues.** (A) Schematic representation (not to scale) of secondary structures in the Sec23 and Sec24 polypeptides based on crystallographic data from *S. cerevisiae* (Bi *et al.*, 2002), and adapted from (Miller *et al.*, 2003). Secondary structural features are noted above. B1-B3 indicates regions involved with forming the cargo recognition B-site on Sec24 (see below). (B) Partial peptide sequence alignments of the interface regions of ScSec23 and ScSec24 with the homologous regions of *T. brucei* orthologues. Residues shared between all three orthologues are boxed in black, while amino acids common to two orthologues are shaded in gray. Alignments were done using Vector NTI software followed by appropriate manual adjustments. Residues in the *S. cerevisiae* sequences that were replaced by corresponding residues in the *T. brucei* sequences to produce the models presented in Fig. S4 are indicated (closed diamonds). (C) Regions comprising the Sec24 cargo-binding B-site from the *S. cerevisiae* Sec24 and both *T. brucei* Sec24 orthologues were aligned using Vector NTI software. Indicated residues (asterisks) are central to forming the basic binding pocket and essential for proper transport of cargo, including p24 proteins, in yeast (Bi *et al.*, 2002; Miller *et al.*, 2003; Mossessova *et al.*, 2003). Notably, while all key B-site residues are conserved in TbSec24.1,

TbSec24.2 lacks a basic arginine at residue 219, replaced by isoleucine, and has a semi-conservative change from leucine to valine at residue 604. These conversions, particularly R219I, are consistent with the two B-sites in the trypanosome Sec24 orthologues having differing specificities for recruitment of membrane cargo to nascent COPII vesicles, which could contribute to GPI-selective cargo loading by the TbSec23.2/TbSec24.1 heterodimer.

**Figure S4. Structural modeling of the *T. brucei* Sec23/Sec24 dimers.** (A) The crystal structure of the *S. cerevisiae* Sec23/Sec24 dimer (Bi *et al*., 2002) in ribbon presentation with shaded space filling background. Arrows are β-strands and cylinders are α-helices. (B) Space filling models of the *S. cerevisiae* subunits rotated to expose the dimer interface. Blue and red indicate positive and negative charge potential, respectively, with color intensity corresponding to charge density. White indicates hydrophobic/neutral regions. Three paired contact surfaces are indicated as a-a', b-b' and c-c'. These crystal data indicate that dimerization is mediated by charge pairing across the dimer interface. (C & D) Models of the TbSec23.1/TbSec24.2 and TbSec23.2/TbSec24.1 dimers. Selective residues from the corresponding regions of the *T. brucei* orthologues (indicated in Fig. S3B) have been substituted into the contact surfaces defined by the *S. cerevisiae* crystal structure. All other residues are from the *S. cerevisiae* structure.

In each case the matched contact surfaces in the modeled *T. brucei* dimers differ in subtle but compensatory ways from the *S. cerevisiae* structure. For instance, a decrease in positive charge in the a-region of TbSec24.2 is compensated by a decrease in negative charge in the a'-region of TbSec23.1 (Panel C). Likewise, a decrease in negative charge in the b-region of TbSec24.1 is compensated for by a decrease in negative charge in the b'-region of TbSec23.2 (Panel D). These changes suggest a co-evolution of matched *T. brucei* subunits such that

dimerization is restricted. For instance, the high positive charge of the a-region of TbSec24.1 is favorable for binding to the negatively charged a'-region of TbSec23.2, but is unfavorable for binding to the relatively hydrophobic a'-region of TbSec23.1. Likewise, the matched relative intensities of the charge pairing across the b-b' regions are most favorable for TbSec24.2/TbSec23.1 (Panel C) and TbSec23.2/TbSec24.1 (Panel D) dimerization. Collectively these subtle but matched changes are likely to account for the exclusive pattern of dimerization observed with the *T. brucei* subunits.

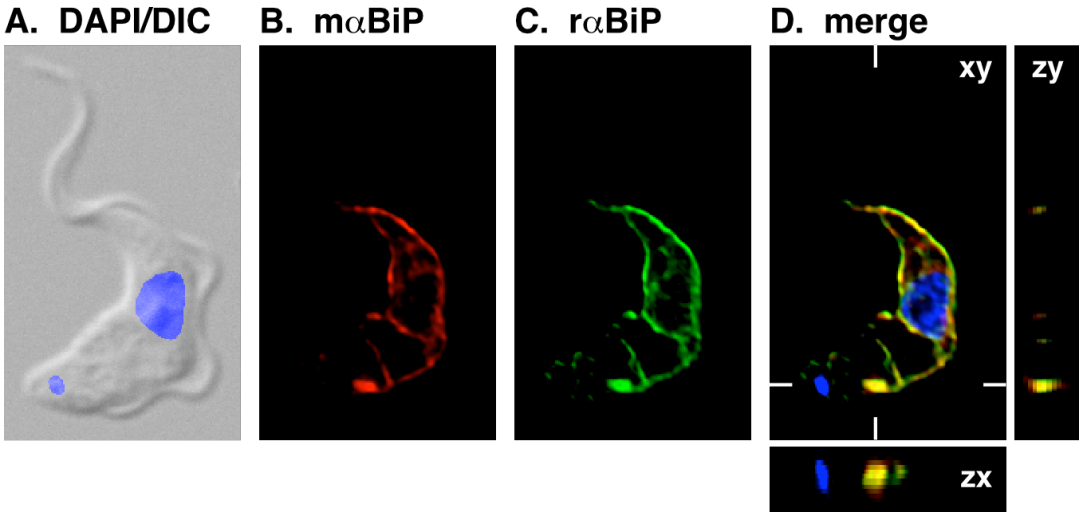


**Figure S1.**

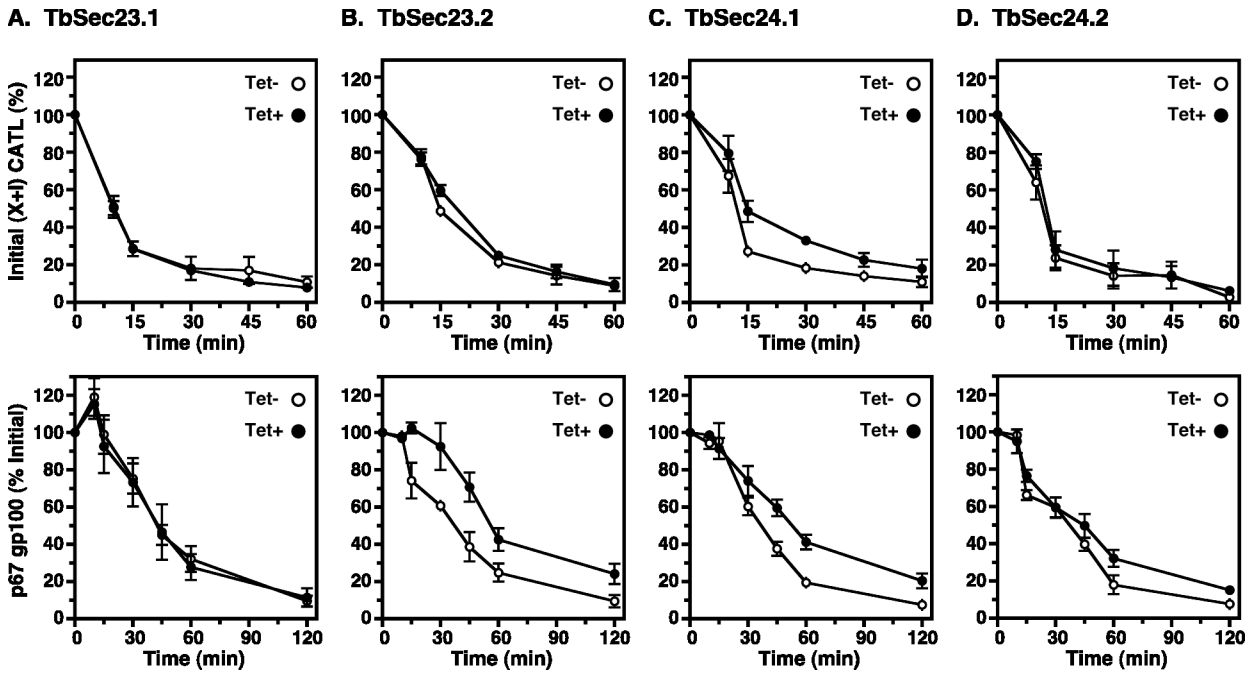
A. TbSec23.1
B. TbSec23.2
C. TbSec24.1
D. TbSec24.2
Initial (X+I) CATL (%)
p67 gp100 (% Initial)
Tet-
Tet+
Time (min)

**Figure S2.**

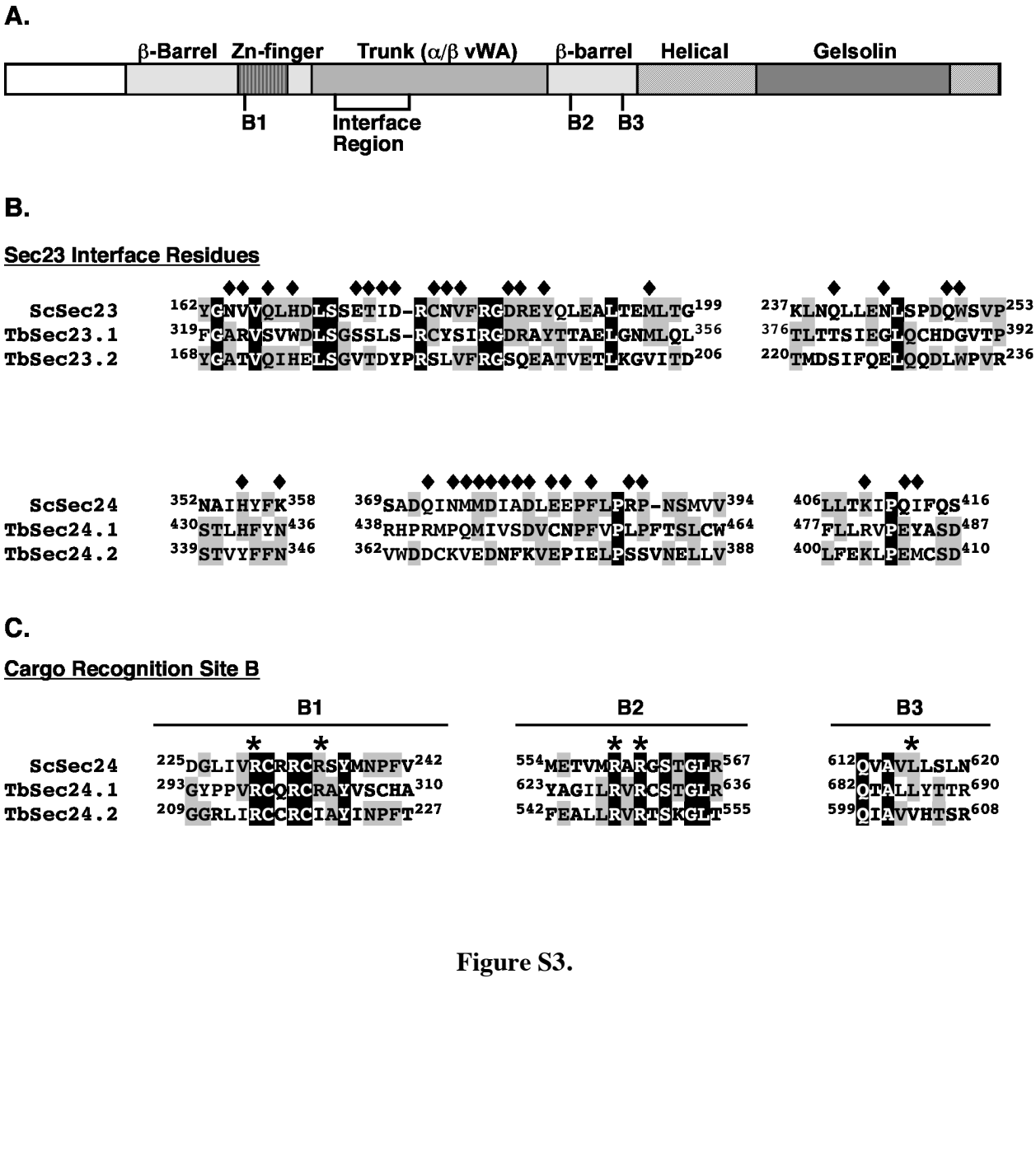
A.
β-Barrel
Zn-finger
Trunk (α/β vWA)
β-barrel
Helical
Gelsolin
B1
Interface Region
B2
B3
B.
Sec23 Interface Residues
ScSec23
TbSec23.1
TbSec23.2
ScSec24
TbSec24.1
TbSec24.2
C.
Cargo Recognition Site B
B1
B2
B3
ScSec24
TbSec24.1
TbSec24.2

**Figure S3.**

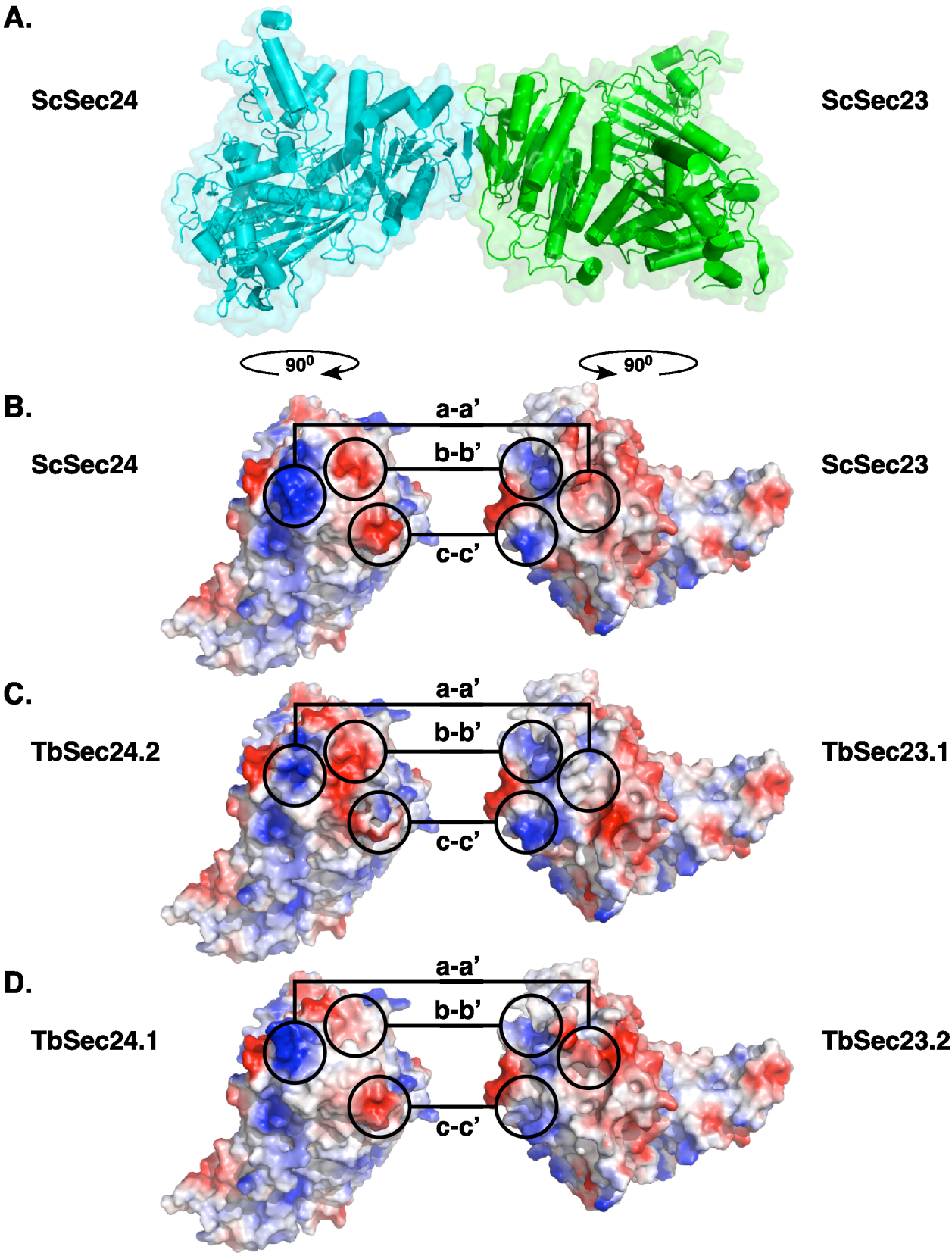
A.
ScSec24
ScSec23
90⁰
90⁰
B.
ScSec24
ScSec23
a-a'
b-b'
c-c'
C.
TbSec24.2
TbSec23.1
a-a'
b-b'
c-c'
D.
TbSec24.1
TbSec23.2
a-a'
b-b'
c-c'

**Figure S4.**